Journal of the European Ceramic Society 19 (1999) 1575–1583

PII: S0955-2219(98)00255-6
0955-2219/99/$ - see front matter

Elastic Properties of High Alumina Cement Castables from Room Temperature to 1600°C

Emmanuel Nonnet,* Nicolas Lequeux and Philippe Boch

Ecole Supérieure de Physique et de Chimie Industrielles 10, rue Vauquelin, 75005 Paris, France

(Received 14 July 1998; accepted 10 October 1998)

Abstract

High-alumina refractory castables with compositions in the systems $CaO–Al_2O_3$ and $CaO–Al_2O_3–SiO_2$ were studied using an ultrasonic technique. The technique allows in-situ, non-destructive measurement of Young's modulus from room temperature to 1600°C. Elastic and dilatometric properties were investigated in relation to phase changes (followed by XRD) and sintering phenomena. The conversion of CAH_{10}, the hydration of still-anhydrous cement phases, and the dehydration of C_3AH_6 and AH_3 are related with events in Young's modulus evolution. Addition of 1 wt% of silica fume strongly decreases the high-temperature mechanical properties. © *1999 Elsevier Science Limited. All rights reserved*

Keywords: refractories, castables, Young's modulus, Al_2O_3, mechanical properties.

1 Introduction

There has been a recent trend among refractories towards replacing bricks by monolithic castables, in particular in the iron and steel industry. Improvements concern starting materials, castable compositions, additives, and installation methods. Improvements also concern the characterisation techniques that are required for the determination of thermal and mechanical properties. In this way, non-destructive evaluation is of special interest for assessing elastic properties of refractory materials.[1,2]

From an industrial point of view, elastic constants (in particular Young's modulus) are parameters whose estimation is required for safe design of loaded structures. From a scientific point of view, elastic constants can be interpreted as second-order derivatives of inter-atomic potentials, which means they bring information on atomic bond strength. In multiphase, polycrystalline materials, elastic constants are sensitive to phase changes and microstructure modifications. Ultrasonic in situ measurement of Young's modulus (or wave velocity) during heat treatments is of interest for studying ceramics[3] and sintering phenomena[4–6] or investigating the high-temperature behaviour of composites[7–9] and shaped[10] or unshaped[11] refractories.

Refractory castables experience large changes from initial setting at room temperature to final use at high temperatures. The present work was aimed at investigating the behaviour of aluminous castables, from room temperature to 1600°C. This required making a dedicated apparatus, which is described first.

2 Ultrasonic Apparatus

One difficulty in high-temperature ultrasonics is that the transducer material (be it piezoelectric or magnetostrictive) loses its properties at the Curie temperature. It is necessary, therefore, to interpose a buffer between the transducer (at room temperature) and the sample under investigation (at high temperature). Buffers are usually shaped as rods.

2.1 Acoustic waves in rods

Let us consider a longitudinal, plane wave, with elastic displacement (u_1) in the direction of propagation (ox_1) for an infinitely long rod of constant cross-section (Fig. 1).[12] If the wavelength is much larger than the diameter of the rod, σ_{11} is the only non-zero component in the stress tensor (σ_{ij}). σ_{12}, σ_{13}, σ_{23}, σ_{22}, and σ_{33} are equal to zero throughout the cross section.

Hooke's law of linear elasticity links stress (σ_{ij}) and strain (ε_{kl}) through the compliance tensor

$$\varepsilon_{11} = \frac{\partial u_1}{\partial x_1} = s_{1111}\sigma_{11}$$

s_{ijkl} being the compliance tensor.

*To whom correspondence should be addressed.

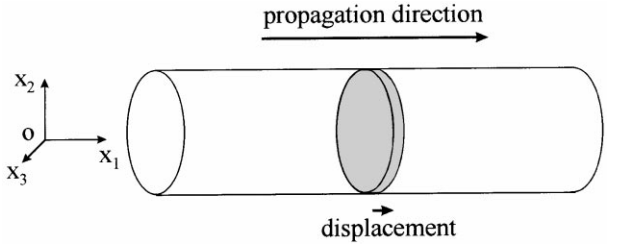

Fig. 1. Propagation of a longitudinal, plane wave in an infinite rod, when $\lambda >> d$ ('beam condition'). Wave front is perpendicular to rod axis.

The fundamental relation of dynamics gives

$$\rho \frac{\partial^2 u_1}{\partial t^2} = \frac{1}{s_{1111}} \frac{\partial^2 u_1}{\partial x_1^2} \quad \rho \text{ being the material density.}$$

The phase velocity (v_b) of the wave (beam velocity) is

$$v_b = \sqrt{\frac{1}{\rho s_{1111}}}$$

If the material is isotropic, the beam velocity becomes

$$v_b = \sqrt{\frac{E}{\rho}} \quad E \text{ being Young's modulus.}$$

The propagation is not dispersive, which means velocity does not depend on frequency. Velocity is independent of the shape of cross section if cross section is constant along the rod. Usual cross sections are circular, square, or rectangular. The beam is guided by the rod, which means there is no beam divergence. For guided-bar mode, acoustic velocity depends on one elastic modulus only (Young's modulus), whereas it depends on two moduli (Young's modulus and shear modulus) in a tridimensional, infinite medium.

2.2 Reflection and transmission

When a plane wave crosses an interface between two different media, partial reflection occurs. The ratio between the reflected and transmitted intensities depends on the reflection and transmission coefficients (r_{12} and t_{12}), defined for waves travelling from medium 1 to medium 2, i, r, and t being put for 'incident', 'reflected', and 'transmitted'

$$r_{12} = \frac{u_r}{u_i} = \frac{Z_1 - Z_2}{Z_1 + Z_2} \qquad t_{12} = \frac{u_t}{u_i} = \frac{2Z_1}{Z_1 + Z_2}$$

For an infinite medium, acoustic impedance (Z expressed in Ray, 1 Ray = 1 kg m^{-2} s^{-1}) is the product of density (ρ) by velocity (v). In beam mode, acoustic impedance is replaced by mechanical impedance, which is the product of acoustic impedance by cross-section area

$$Z = \rho v S \quad S \text{ being cross section area.}$$

2.3 Acoustic equipment

2.3.1 Frequency

The refractory castables under study exhibit a coarse microstructure where heterogeneities can be as large as 1 mm. For averaging the properties, it is necessary that the cross-section diameter (d) be at least 10 times larger than the largest heterogeneity. This condition leads to $d \geq 10$ mm, which requires a minimum wavelength to fulfil the beam mode

$$\lambda = \frac{v}{f} \gg d$$

The acoustic velocity in refractory castables ranges from 2500 to 6000 m s^{-1}, depending on heat treatment. Taking the minimum of 2500 m s^{-1}, a frequency of 40 kHz leads to a wavelength of $\lambda = 63$ mm, which fulfils the beam mode requirement. Another difficulty with castables is their high acoustic attenuation, particularly at high temperatures. Since attenuation dramatically increases with frequency, this is another reason for choosing a low frequency of 40 kHz.

Magnetostrictive transducers are preferred in low-frequency applications. The transducer conception was as follows

i. A magnetostrictive rod is polarised by an axially-applied constant magnetic field, generated by tore-shape permanent magnets.
ii. The transducer is excited by an electric signal circulating within a coil wrapped around the rod.
iii. The central frequency f_c of the ultrasonic pulse which propagates from the magnetostrictive rod to the acoustic buffer depends on the rod length

$$f_c = \frac{v_m}{2L_m}$$

v_m being the sound velocity in the rod and L_m the length of the rod.

iv. The transducer acts as both transmitter and receiver (echo mode). The echo mode involves one buffer–sample interface, whereas the transmission mode involves two interfaces (buffer–sample and sample–buffer).

2.3.2 Impedance matching; wave guide

A low frequency means wide pulses, hence possible overlap between successive echoes. This problem is minimised when the pulse is narrow, which requires good matching between the magnetostrictive rod and the buffer. If matching is poor, the reflection coefficient is high and the pulse is widened by reflections at the inside of the magnetostrictive rod.

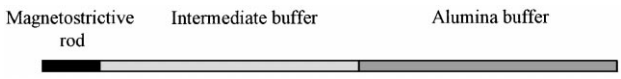

Fig. 2. Ultrasonic wave guide. The three rods have same diameter.

The buffer must resist high temperatures ($\geq$ to 1600°C) and oxidising atmospheres, which precludes from using non-oxide materials. High-purity, dense alumina offers high strength, good refractoriness, excellent thermal stability, and low acoustic attenuation. However, its acoustic impedance is much higher than that of the magnetostrictive material.

Acoustic matching between two materials with so dissimilar acoustic impedances is a challenge. The best results were obtained by inserting an intermediate buffer between the magnetostrictive rod and the alumina buffer (Fig. 2).

Figure 3 shows an echo pattern for a sample-free configuration, that is for the wave guide only. The working window, which is the domain where the echoes caused by a sample have to occur, is delimited by the time interval between echoes A_1 and A_2. By using an intermediate buffer with sufficient length, one can reject the second echo that arises at the intermediate–alumina buffers interface (IA_2) at the exterior of the working window, which avoids interference with sample echoes.

An echo sequence for a sample-coupled configuration is represented in Fig. 4. The echoes of interest for determining the sample acoustic velocity are the first alumina back side echo (A_1) and the first sample back side echo (S_1). Moreover, the buffer method allows the determination of reflection coefficient and acoustic attenuation provided that the second sample back-side echo (S_2) can be monitored.[13] The acoustic velocity (v_b) is expressed as $v_b = \frac{2L}{\tau}$ τ being the travelling time between echoes A_1 and S_1 and L the sample length.

The length of the sample must be such that the first back-side echo does not overlap with the alumina echoes. This criterion has to be respected throughout the experiment, although the acoustic properties change with temperature. All parameters combine to restrict measurable travelling times to values ranging from 55 to 105 μs.

2.4 Travelling time determination

There are various methods for measuring the travelling time between two broadband signals. The direct method of measuring the interval between homologous points on successive echoes is very sensitive to echo distortions. Although quite old,[14] the more accurate echo-overlap method is still frequently used. Methods based on Fourier analysis give better results than the echo-overlap method when the echoes are distorted, attenuated,[15] or even shifted.[16]

We used a Fourier method, where the travelling time is determined from the position of the maximum of the envelope of the cross-correlation function of two relevant echoes. The method allows the in-situ study of changes in travelling time during thermal treatments. Calculation is done in real-time. The acquisition and calculation rates have values that allow the registration of 17 travelling time data per min, which puts an upper limit of 3–4°C min^{-1} for the heating rate. The scattering of data due to electronics yields an absolute accuracy of travelling time of 0·3 μs.

2.5 Assembly description

Figure 5 is a schema of the assembly. The vertical configuration minimises the creep of alumina buffer and sample. The sample is located at the top of

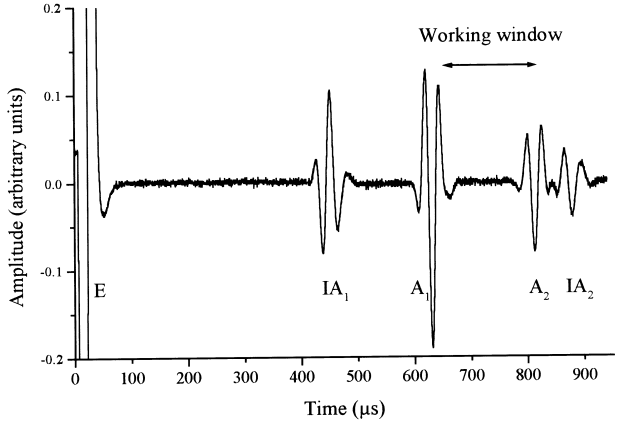

Fig. 3. Excitation is *E*, first and second echoes at the intermediate–alumina buffer interface are IA_1 and IA_2, first and second echoes at the free end of the alumina rod are A_1 and A_2.

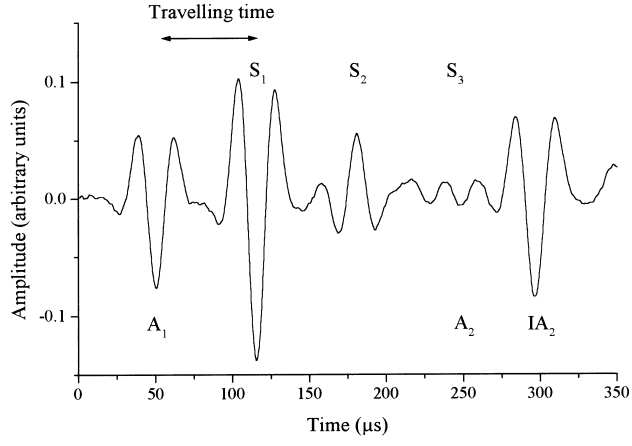

Fig. 4. Working window for a sample-coupled configuration (FFT filtered signal). First and second echoes at the alumina–sample interface are A_1 and A_2, second echo at the intermediate–alumina buffers interface is IA_2, first, second, and third sample back-side echoes are S_1, S_2 and S_3, respectively.

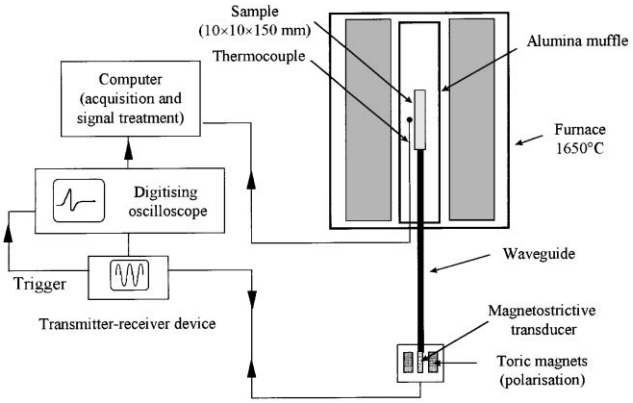

Fig. 5. Apparatus for in-situ dynamic determination of Young's modulus of refractory materials (20–1650°C, in air).

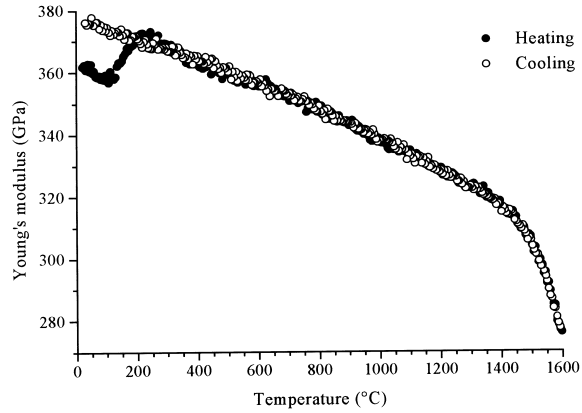

Fig. 6. Young's modulus of dense polycrystalline alumina (heating/cooling rate = 3°C min^{-1}).

the wave guide, with the advantage that all the interfaces (sample–alumina, alumina–intermediate buffer, and intermediate buffer–transducer) are in compression, which helps avoiding interface cracking. The sample is heated by a 6-kW tubular furnace ($LaCrO_3$ heating elements). An alumina muffle (∅ 56 mm) prevents the sample from being polluted by vaporisation of heating elements. The thermocouple is located in the middle of the sample and at 1 cm from the muffle. The sample length must not exceed ≈150 mm to ensure reasonable thermal homogeneity. At 1200°C, the temperature gradient along the sample is ≈25°C, with a transverse temperature difference between the sample and the muffle of ≈15°C.

2.6 Interface coupling

Although acoustic coupling between sample and buffer can be obtained by simple contact,[6] it is much safer to glue the sample with the buffer.

At room temperature, there are various possible binders. An organic glue was used to stick the magnetostrictive rod with the intermediate buffer. However, problems are encountered with temperature-resistant binders, which have to endure high-temperatures, expansion mismatch between alumina and sample, and corrosion effects. The best results were obtained with a high-temperature adhesive that resists temperatures of 1600°C. The binder thickness must be as thin as possible to minimise interfacial acoustic phenomena.

To assess the coupling properties of the binder, we carried out experiments on alumina (Degussit AL23), a material known to be free from structural transitions over the whole temperature range. The Young's modulus versus temperature relationship is[17]

$$E(T) = E_0 - BT\exp\left(-\frac{T_0}{T}\right)$$

For dense, high-purity, polycrystalline alumina, E_0, B, and T_0 are 350–400 GPa, 0·05 GPa °C^{-1}, and 310 K, respectively. The $E(T)$ curve can be approximated by a straight line from 20 to 1400°C.

The alumina sample (6·1 mm-diameter rod) was glued on the alumina buffer using the high-temperature adhesive. After 24 h soak at room temperature, the system was heated to 1600°C, then cooled to room temperature (heating/cooling rates = 3°C min^{-1}). Figure 6 shows a regular decrease in E when T increases, with an event in the low side of the heating curve. This event, which corresponds to a travelling time drop of ≈ 1.3 μs, is due to the binder. In fact, the binder supplier indicates that a treatment of 2 h at 120°C must complete the room-temperature soak. The difficulty here is that the hydrated cement in the castables under study also begins to transform at about 120°C. The solution was of gently heating the alumina buffer at a distance of ≈50 mm from the interface, in order to heat the binder by thermal conduction through the buffer without damaging the sample. This procedure reduces the intensity of the time drop from 1·3 to 0·6 μs.

The rapid decrease in Young's modulus at temperatures superior to 1400°C can be attributed to viscous phenomena due to grain boundary segregation of impurities or sintering additives. The absence of hysteresis on the heating/cooling plots indicates that the binder works perfectly.

Table 1. Castables composition (wt%)

Castable	*C12·5 (%)*	*C37·5 (%)*	*C12·5S1 (%)*
Cement (SECAR 71)	12·5	37·5	Similar to C12·5 but with 1% silica fume
Reactive alumina (CT 3000 SG)	37·5	12·5	
Tabular alumina (14–28 mesh)	50	50	
Silica fume additive	—	—	
Darvan 7S	0·1	0·1	
Citric acid	0·04	0·04	

3 Materials

Three castable compositions were used, labelled C12·5, C37·5, and C12·5S1 (Table 1). The high-alumina cement (SECAR 71 Lafarge Aluminates, $d_{50} = 10\ \mu m$) consists mainly of calcium mono-aluminate (CA), calcium di-aluminate (CA_2), and α-alumina. The filler was reactive alumina (CT 3000SG Alcoa, $d_{50} = 0{\cdot}6 - 0{\cdot}8\ \mu m$). The cement plus the reactive alumina constitute the binding phase. Tabular alumina (T60 Alcoa, $d_m \approx 0{\cdot}8$ mm) was used as grog. The grog relative content was of 50 wt% in all castables. Castable C12·5S1 was obtained by adding 1 wt% of silica fume to castable C12·5.

The castables were prepared by vigorously mixing the dry powders, then adding deflocculant-containing water and mixing for 4 min. Darvan 7S was used as deflocculant and citric acid as deflocculant and retarder. The water-to-solid ratio was 0·1 for all compositions. $150\times10\times10$ mm samples were then cast and vibrated. The cure was of 7 days at 20°C in water saturated atmosphere. At this temperature, the hydrated phase that develops is crystalline mono-calcium aluminate deca-hydrate (CAH_{10}).

4 Results and Discussion

Heat treatment yields changes in both Young's modulus (E) and density (ρ). If the dimensional changes are isotropic, one can write

$$E(T) = E'(T)\frac{l_0 m(T)}{l(T) m_0}$$

with

$$E'(T) = \rho_0 \left(\frac{2l_0}{\tau(T)}\right)^2$$

m, l, and τ being the sample mass, the sample length, and the travelling time, respectively, the subscript zero referring to room temperature and T being temperature.

Thermogravimetry [to determine $m(T)$] and dilatometry [to determine $l(T)$] experiments were carried out using the same heating rate as Young's modulus experiments. The weight loss varies from 6 to 9% and the expansion/shrinkage effects do not exceed 1–2% (Fig. 7). Figure 8 shows the curves of Young's modulus (corrected from the density/dilation changes) versus temperature for castables C12·5 and C12·5S1.

4.1 Cement dehydration; conversion of CAH_{10}

Experiments were carried out using silica-free samples.

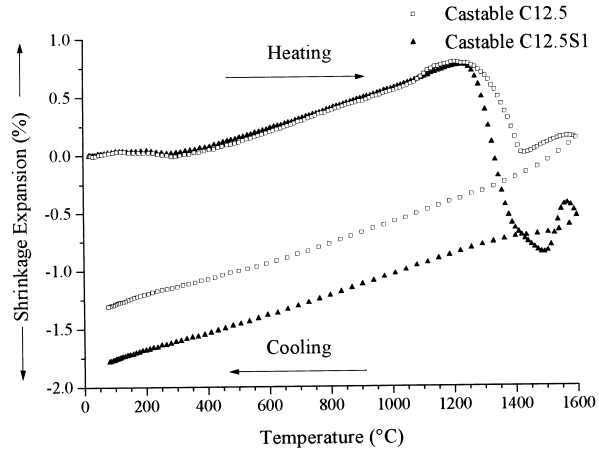

Fig. 7. Dimensional changes versus temperature for castables C12·5 and C12·5S1. Heating rate = 3°C min^{-1}. Furnace cooling. Sample dimensions: $10\times10\times30$ mm.

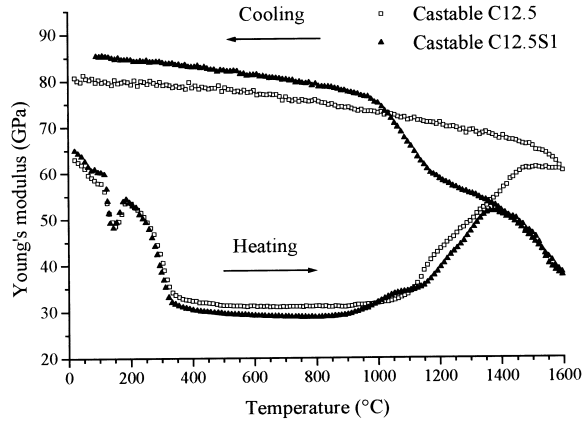

Fig. 8. Young's modulus versus temperature for castables C12·5 and C12·5S1. Heating/cooling rate = 3°C min^{-1}. Sample dimensions: $10\times10\times150$ mm.

In high-alumina cements hydrated at room temperature, the main hydrate is CAH_{10}. When temperature increases, CAH_{10} partially dehydrates (at $\approx$ 110°C), then the residue converts to a mixture of tricalcium aluminate hydrate (C_3AH_6) and gibbsite (AH_3) (at $\approx$ 120°C). This suggests that the transient drop of modulus observed in the low-temperature side of the curves shown in Fig. 10 is caused by the conversion of CAH_{10}. At $T \geq 300$°C, dehydration of C_3AH_6 and AH_3 results in low moduli, whatever the composition.

As far as we know, there were no published data on the elastic effects associated with the conversion of CAH_{10} and it was interesting, therefore, to study the phenomenon in a detailed manner.

i. A first point was to check whether the change in modulus was not an experimental artefact caused by modifications in the coupling binder between the wave guide and the sample. To discount this possibility, we conducted a test on a cement-rich sample (castable C37·5) that had been treated at 110°C for 64 h to vaporise

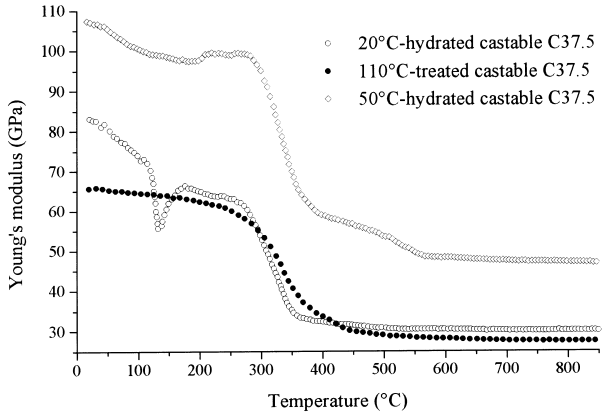

Fig. 9. Young's modulus versus temperature for castables C (heating rate = 3°C min^{-1}). The transient loss of modulus is observed on the 20°C-hydrated material but is not observed on the 50°C-hydrated and 110°C-treated materials.

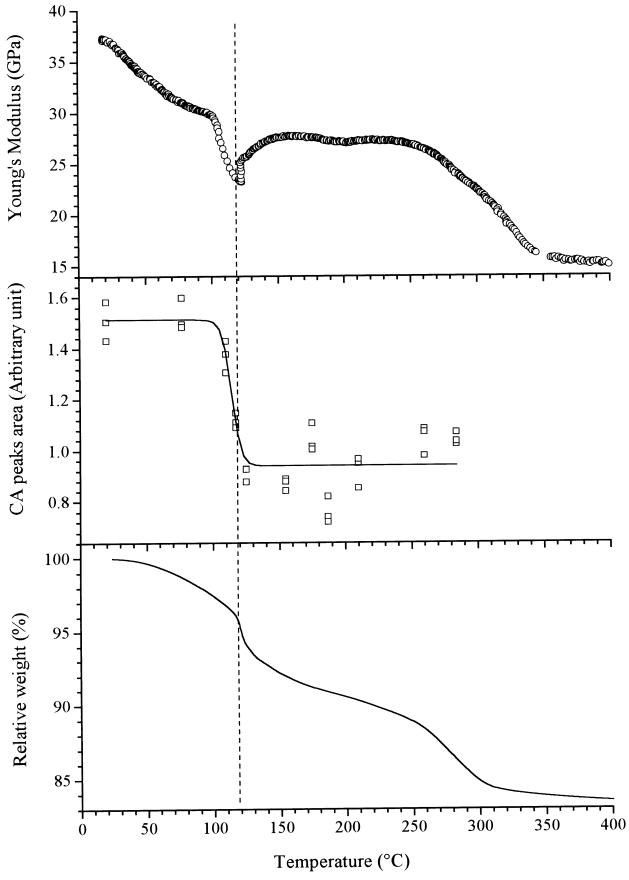

Fig. 10. 75% SECAR 71 + 25% reactive alumina material. (a) Young's modulus versus temperature (uncorrected for weight loss and dilation); (b) relative content of CA in quenched samples versus quenching temperature; (c) weight loss versus temperature. (All tests were conducted at heating rate of 3°C min^{-1}.)

excess water and convert CAH_{10} to C_3AH_6 and AH_3, before to be coupled with the wave guide. Fig. 9 shows that the Young's modulus curve now observed is perfectly regular, which confirms that the event observed on untreated castables is not an artefact due to the binder.

ii. A second point was to check whether a castable that had been hydrated at 50°C (i.e. at a temperature where C_3AH_6 forms) leads to an event-free curve. Fig. 9 shows this is the case. The fact that the room temperature modulus is higher in the 50°C-hydrated castable than in the 20°C-hydrated one is due to a higher degree of hydration in the former than in the latter. XRD experiments were performed on both materials. They show that the fraction of CA that hydrates at 50°C is about twice as the fraction that hydrates at 20°C.

iii. The third point was to study the conversion of CAH_{10} in a grog-free material constituted only of 75% SECAR 71 plus 25% reactive alumina (water-to-solid ratio of 0·17, cure for 48 h at 20°C in water saturated atmosphere). To improve the precision of temperature measurement during Young's modulus evolution (heating rate = 3°C min^{-1}), the thermocouple was directly stuck onto the surface of the sample [Fig. 10(a)]. XRD experiments (Cu-K_α radiation, Philips 1710 diffractometer) were conducted on bulk samples air-quenched from temperatures inferior-to and superior-to the temperature of conversion. The CA relative content was semi-quantitatively determined (accuracy $\approx$ 10%) by measuring the XRD peak area of (123) and (220) reflections of CA, normalised by (116) reflection of alumina [Fig. 10(b)]. The weight loss of a bulk sample was also measured [Fig. 10(c)].

The conversion of CAH_{10} to $C_3AH_6 + AH_3$ occurs through the following reaction

$$3CAH_{10} \rightarrow C_3AH_6 + 2AH_3 + 18H \qquad (1)$$

Reaction (1) involves a dissolution/reprecipitation mechanism,[18] whose rate increases with temperature.[19] For an experiment carried out at a fixed heating rate, one has to take into account that CAH_{10} partially dehydrates to give CAH_x in the temperature range where the conversion occurs ($\sim$ 100°C). The value of x is very sensitive to experimental conditions. At 100°C, for instance, x is 3·5 for constant-temperature dehydration whereas it is 6·5 for 5°C min^{-1} dynamic dehydration.[20] The conversion reaction can now be written as

$$3CAH_x \rightarrow C_3AH_6 + 2AH_3 + (3x-12)H \; (x > 4) \qquad (2)$$

The water loss can be followed using thermogravimetry, as shown in Fig. 10(c).

All results unambiguously confirm that the change in modulus is associated with the conversion of CAH_{10}. A very interesting point is that the loss of mechanical properties[21] induced by the conversion is only transient in this case of low

water-to-cement ratio materials. After the drop in modulus, there is an increase, which can be attributed to hydration of the still anhydrous CA by the water that is released by the conversion process. This is confirmed by Fig. 10(b) which shows that the decrease in the CA content is accompanied by the increase in modulus. This means that these castables can compensate the effects of the conversion and recover certain mechanical properties by further hydration of anhydrous phases of the cement.

By mechanical properties, we mainly mean elastic modulus. However, our experiments on the castables (not presented here) have shown that there is a strong correlation between elastic modulus (E) and mechanical strength (σ_f). It is known that in brittle materials $\sigma_f \sim E^{1/2}c^{-1/2}$ if c is the equivalent size of critical defects. All other things being constant, an increase in E yields an increase in σ_f.

4.2 Sintering

After dehydration (Fig. 8), the modulus of castable C12·5 rests at a low value until sintering starts (at $T > 900°C$), after what it increases, first slowly and then (at $T > \approx 1100°C$) faster. Sintering is accompanied by phase changes, with development of the strong atomic bonds that are characteristic of ceramic compounds.

Phase changes (Fig. 11) were followed by XRD experiments on furnace cooled samples. The XRD peaks area were normalised by the (116) reflection of alumina (Cu-K_α radiation, Philips-1710 diffractometer). However, reactions between cement phases and reactive alumina do not allow the results to be quantitative.

4.2.1 Phase change

CA is the first crystalline phase that develops (at $T \approx 900°C$), then CA reacts with alumina to give CA_2 (at $T \approx 1100°C$). CA_6 becomes the main calcium aluminate phase in castable C12·5 treated at high temperatures ($T > 1500°C$). The reaction between calcium aluminates and alumina mainly involves the fine alumina, whereas the coarse alumina remains virtually inactive. In castable C12·5, the composition of the binding phase is close to that of CA_6. SEM observations and X-ray microanalysis (not presented here) on samples sintered at 1600°C confirm that the binding phase is constituted of tabular crystals of CA_6.

4.2.2 Dilatometric behaviour

Between 100 and 300°C the thermal expansion of castable C12·5 is balanced by the shrinkage due to dehydration (Fig. 7). From ≈ 300 to $\approx 1100°C$, the thermal expansion is the only active expansive process. At higher temperatures, two competitive phenomena develop, namely (i) expansion due to formation of CA_2 and CA_6 and (ii) shrinkage due to sintering. The formation of CA_2 from CA and A, which starts at $\approx 1100°C$, is expansive.[22] The formation of CA_6 from CA_2 and A at $\approx 1450°C$ is expansive too.[23] This expansion observed in corundum concrete is mainly due to anisotropic growth of tabular crystals.[24] Expansion effects due to phase changes compete with densification shrinkage and can even overpass it, as shown in castable C12·5 at $T > 1400°C$.

4.2.3 Young's modulus behaviour

It is a general rule that all other things being constant a porosity decrease results in a Young's modulus increase. The increase in modulus of castable C12·5 begins at a temperature inferior to 1000°C, whereas densification does not develop below 1200°C (Fig. 7). This indicates that cohesion depends on parameters such as changes in the binding phase and growth of sintering necks[25] and particle size.[26] The changes in the slope of the $E = f(T)$ curve at $\approx 1150°C$ and at $\approx 1450°C$ must be related to the formation of CA_2 and CA_6, respectively.

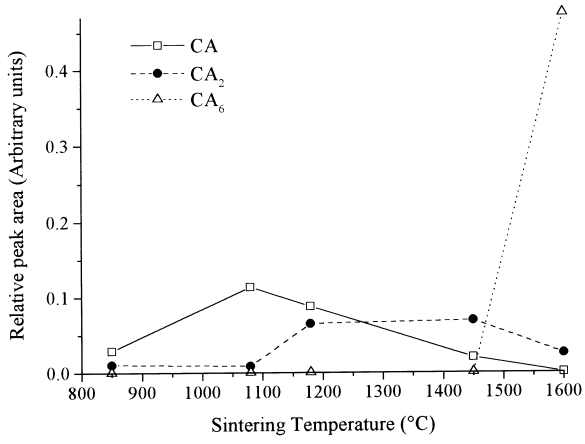

Fig. 11. Estimation of calcium aluminate content (XRD data) versus sintering temperature in castable C12·5.

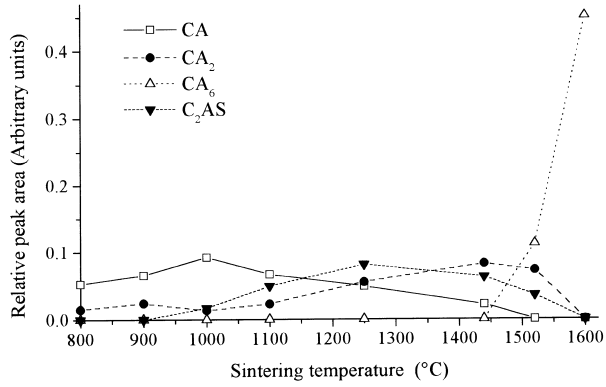

Fig. 12. Estimation of calcium aluminates and gehlenite content (XRD data) versus sintering temperature for castable C12·5S1.

4.3 Influence of silica fume addition

Comparison between castables C12·5 and C12·5S1 shows the influence of 1 wt% of silica fume addition.

4.3.1 Phase change

Figure 12 shows that the presence of silica does not significantly affect the high temperature sequence of formation of the silicon-free calcium aluminates. The only silicon-containing crystalline phase we observed are gehlenite (C_2AS) and quartz (traces). C_2AS is out of equilibrium because it is not part of the subsystem CA_6–A–CAS_2 (CAS_2 = anorthite) where the binding phase is located. C_2AS is observed after heat treatment at $\approx$ 900°C. No crystalline silicon-containing phase (except residual quartz) can be observed in materials furnace cooled from 1600°C. It must be noticed that the furnace we used leads to rather high cooling rate ($\approx 15°C\,min^{-1}$ from 1600 to 1000°C). This means that high temperature phases are expected to be quenched.

4.3.2 Dilatometric behaviour

Comparison between the dimensional changes of castables C12·5 and C12·5S1 shows that both castables exhibit the same behaviour up to 1100°C (Fig. 7). At higher temperatures, the silica-containing material shows three differences by comparison with its silica-free counterpart, namely: (i) sintering shrinkage begins at a slightly lower temperature and is larger, (ii) the weak expansion associated with the formation of CA_2 is masked by the shrinkage, and (iii) the large expansion at high-temperature ($\approx$1450°C) which is associated with the formation of CA_6 is more visible, because the more precocious shrinkage does not mask it.

4.3.3 Young's modulus behaviour

At $T <\approx$ 900°C, the castable with 1 wt% of silica fume exhibits about the same behaviour as its silica-free counterpart (Fig. 8). In the high-temperature domain, however, there are three differences between the two materials. Firstly, the presence of silica leads to an earlier increase in modulus, which is associated with viscous sintering, as observed in most silicon-containing ceramics. Secondly, silica causes a dramatic decrease in modulus at temperatures superior to 1350–1400°C, which can be associated with development of non-equilibrium liquid at 1380°C, eutectic point of the subsystem CA_6–C_2AS–CAS_2. This agrees with the report of Kriechbaum *et al.*[27] that even a small content of silica fume dramatically decreases the mechanical properties of high alumina castables, due to considerable enhancement of viscous flow creep. Thirdly, the high-temperature side of the cooling curve of castable C12·5S1 shows an important increase between 1200 and 1000°C, which can be caused by the progressive solidification of supercooled glassy phase. Another possible explanation might be devitrification. However, the room-temperature XRD data do not indicate the presence of silica-containing phase (except residual quartz) in materials sintered at 1600°C.

5 Conclusion

The acoustic apparatus developed is well adapted to the non-destructive, in-situ study of elastic changes in castables submitted to heat treatment. The method exhibits high reproducibility and sensitivity. All phase changes are detected, with particular mention of conversion of CAH_{10}, reactions between calcium aluminates and alumina, and liquid phase formation in the material that contains silica fume. The ability of high-alumina castables with low water-to-cement ratio to recover their initial elastic modulus after the conversion of CAH_{10} deserves special mention.

Acknowledgements

The study was supported by Lafarge with approval of A. Capmas and B. Espinosa (Lafarge Aluminates). The authors gratefully acknowledge Drs K. Scrivener and H. Fryda (Lafarge Research Centre) for continuous assistance. They thank Professor C. Gault and Dr M. Huger (Ecole Nationale Supérieure de Céramique Industrielle), whose expertise in high-temperature acoustic experiments has been most appreciated, and Professor D. Royer (Ecole Supérieure de Physique et de Chimie Industrielles), whose help has been invaluable. K. Weulersse is also thanked for her assistance.

References

1. Bell, D. A., Non-destructive testing of refractories. *Br. Ceram. Trans. J.*, 1989, **88**, 133–137.
2. Crecraft, D. I., Ultrasonic instrumentation: principles, methods and applications. *J. Phys. E: Sci. Instrum.*, 1983, **16**, 181–189.
3. Gault, C., Ultrasonic non destructive evaluation of microstructural changes and degradation of ceramics at high temperature. In *Materials Research Society Symposium Proceedings*, Vol. 142, ed. J. Holbrook and J. Bussiere. Materials Research Society, Pittsburgh, PA, 1989, pp. 263–274.
4. Gieske, J. H. and Frost, H. M., Technique for measuring ultrasonic velocity and attenuation changes in attenuative materials at temperature such as during sintering process. *Rev. Sci. Instrum.*, 1991, **62**, 3056–3060.
5. Telschow, K. L., Walter, J. B. and Garcia, G. V., Laser ultrasonic monitoring of ceramic sintering. *J. Appl. Phys.*, 1990, **68**, 6077–6082.

6. Komarenko, P., Messler, R. W. and Scarton, H. A., Ultrasonic in situ monitoring of sintering in alumina. *Int. J. Powder Metall.*, 1994, **30**, 67–76.
7. Lamidieu, P. and Gault, C., Endommagement et microstructure de composites céramique-céramique sollicités thermiquement. *Revue Phys. Appl.*, 1988, **23**, 201–211.
8. Cutard, T., Fargeot, D., Gault, C. and Huger, M., Ultrasonic measurements of Young's modulus in dog-bone-shaped samples subjected to a tensile stress. *J. Appl. Phys.*, 1994, **76**, 126–132.
9. Huger, M., Fargeot, D. and Gault, C., Ultrasonic characterization of oxidation mechanisms in Nicalon/C/SiC composites. *J. Am. Ceram. Soc.*, 1994, **77**, 2554–2560.
10. Gault, C., Platon, F. and Le Bras, D., Ultrasonic measurements of Young's modulus of Al_2O_3-based refractories at high temperatures. *Mat. Sc. and Engg*, 1985, **74**, 105–111.
11. Lamidieu, P. and Gault, C., Improved ultrasonic measurement of Young's modulus at high temperature in composite ceramics: application to refractory concretes. *Mat. Sc. and Engg*, 1986, **77**, L11–L15.
12. Royer, D. and Dieulesaint, E., *Ondes élastiques dans les solides tome 1, Propagation libre et guidée*. Masson, Paris, 1996, pp. 292–295 (in French).
13. Papadakis, E. P., Ultrasonics measurements methods. In *Physical Acoustics*, vol. 19, ed. R. N. Thurston and A. D. Pierce. Academic Press, New York, 1990, pp. 107–155.
14. Papadakis, E. P., Ultrasonics measurements methods. In *Physical Acoustics*, vol. 19, ed. R. N. Thurston and A. D. Pierce. Academic Press, New York, 1990, pp. 81–106.
15. Hull, D. R., Kautz, H. E. and Vary, A., Measurement of ultrasonic velocity using phase-slope and cross correlation methods. *Mater. Eval*, 1985, **43**, 1455–1460.
16. Cutard, T., Fargeot, D., Gault, C. and Huger, M., Time delay and phase shift for ultrasonic pulses using autocorrelation methods. *J. Appl. Phys*, 1994, **75**, 1909–1913.
17. Wachtman, J. B., Tefft, W. E., Lam, D. G. and Apstein, C. A., Exponential temperature dependence of Young's modulus for several oxides. *Phys. Rev*, 1961, **122**, 1754–1759.
18. Bradbury, C., Callaway, P. M. and Double, D. D., The conversion of high alumina cement/concrete. *Mat. Sc. and Engg*, 1976, **23**, 43–53.
19. Midgley, H. G., The mineralogy of set high-alumina cement. *Trans. Brit. Ceram. Soc*, 1967, **66**, 161–187.
20. Buttler, F. G. and Taylor, H. F. W., Monocalcium aluminate decahydrate: unit cell and dehydration behaviour. *Il Cemento*, 1978, **3**, 147–152.
21. Midgley, H. G. and Midgley, A., The conversion of high alumina cement. *Mag. Concr. Res.*, 1975, **27**, 59–77.
22. Criado, E. and De Aza, S., Calcium hexaluminate as refractory material. In *Unified International Technical Conference on Refractories Proceedings*, Aachen 1991. Stahl, Eisen, Germany, 1992, pp. 566–574.
23. Criado, E., Estrada, D. A. and De Aza, S., Estudio Dilatometrico sobre la formacion de dialuminato y hexaluminato de calcio en cementos y hormigones refractarios. *Bol. Soc. Esp. Ceram. Vidr.*, 1976, **15**, 319–321.
24. Figusch, V., Kanclir, E. and Liska, J., Dilatation des bétons réfractaires légers de corindon dans l'intervalle de température de1400–1500°C. *Bull. Soc. Fr. Ceram.*, 1980, **129**, 47–53.
25. Martin L. P., Rosen M., Correlation between surface area reduction and ultrasonic velocity in sintered zinc oxide powders. *J. Am. Ceram. Soc.*, 1997, **80**, 839–846.
26. Takahashi, N., Ishikawa, M. and Watanabe, K., The deformation behavior of low cement castables. *Taikabutsu Overseas*, 1997, **17**, 96.
27. Kriechbaum, G. W., Gnauck, V. and Routschka, G., The influence of SiO2 and spinel on the hot properties of high alumina low cement castables. 37th Colloquium on Refractories, Aachen, 1994, pp. 150–159.